Identification and Dynamics of a Heparin-Binding Site in Hepatocyte Growth Factor[†]

Hongjun Zhou,[‡] José R. Casas-Finet,[§] R. Heath Coats,[‡] Joshua D. Kaufman,[∥] Stephen J. Stahl,[∥] Paul T. Wingfield,[∥] Jeffrey S. Rubin,[⊥] Donald P. Bottaro,[⊥] and R. Andrew Byrd*[,‡]

Macromolecular NMR Section, ABL-Basic Research Program, and AIDS Vaccine Program, SAIC Frederick, NCI-Frederick Cancer Research and Development Center, Frederick, Maryland 21702-1201, Protein Expression Laboratory, National Institute of Arthritis and Musculoskeletal and Skin Diseases, Bethesda, Maryland 20892-2775, and Laboratory of Cellular and Molecular Biology, Division of Basic Science, National Cancer Institute, Bethesda, Maryland 20892-4255

Received April 14, 1999; Revised Manuscript Received July 20, 1999

ABSTRACT: Hepatocyte growth factor (HGF) is a heparin-binding, multipotent growth factor that transduces a wide range of biological signals, including mitogenesis, motogenesis, and morphogenesis. Heparin or closely related heparan sulfate has profound effects on HGF signaling. A heparin-binding site in the N-terminal (N) domain of HGF was proposed on the basis of the clustering of surface positive charges [Zhou, H., Mazzulla, M. J., Kaufman, J. D., Stahl, S. J., Wingfield, P. T., Rubin, J. S., Bottaro, D. P., and Byrd, R. A. (1998) *Structure 6*, 109−116]. In the present study, we confirmed this binding site in a heparin titration experiment monitored by nuclear magnetic resonance spectroscopy, and we estimated the apparent dissociation constant (K_d) of the heparin−protein complex by NMR and fluorescence techniques. The primary heparin-binding site is composed of Lys60, Lys62, and Arg73, with additional contributions from the adjacent Arg76, Lys78, and N-terminal basic residues. The K_d of binding is in the micromolar range. A heparin disaccharide analogue, sucrose octasulfate, binds with similar affinity to the N domain and to a naturally occurring HGF isoform, NK1, at nearly the same region as in heparin binding. ^{15}N relaxation data indicate structural flexibility on a microsecond-to-millisecond time scale around the primary binding site in the N domain. This flexibility appears to be dramatically reduced by ligand binding. On the basis of the NK1 crystal structure, we propose a model in which heparin binds to the two primary binding sites and the N-terminal regions of the N domains and stabilizes an NK1 dimer.

Hepatocyte growth factor (HGF)[1] is a potent mitogen, motogen, and morphogen which targets a wide range of cells (*1*, *2*). Extensive studies have established that HGF mediates epithelial−mesenchymal interactions and somatic cell migration, which are crucial for the development, maintenance, and regeneration of various tissues and organs (*3*). HGF has been implicated in many human diseases, including acute and chronic renal failure, liver fibrosis/cirrhosis, and cancer (*3*, *4*). Mature HGF consists of an N-terminal (N) domain and four "kringle" domains (K1−K4) in its α-chain and a serine protease homology domain in its β-chain (*2*). The N domain contains two disulfide linkages which are also found in the N-terminal domains of plasminogen and macrophage stimulating protein. The β-chain has no protease activity due to residue changes in the catalytic triad. The N and K1 domains of HGF appear to be involved in binding to the receptor of HGF, the proto-oncogene product c-Met (*5*). Experiments suggest that the receptor-binding characteristics of HGF are primarily localized in K1 (*6*, *7*; J. S. Rubin and D. P. Bottaro, unpublished results).

In addition to high-affinity binding to c-Met, HGF also binds to glycosaminoglycans, such as heparan sulfate (HS), associated with the membrane and extracellular matrix (*8*−*10*). HS is similar in composition and structure to heparin, and both bind to HGF with similar affinity. The effect of exogenous heparin on HGF signaling resembles that observed in fibroblast growth factor (FGF) signaling (*11*−*13*). Heparin is able to enhance the biological function of HGF under certain conditions, possibly by stimulating ligand and receptor dimerization (*10*, *14*, *15*), although it also has been observed to inhibit HGF activity in other circumstances (*16*). The apparent dissociation constant (K_d) was estimated to be in the nanomolar range (1−50 nM) for HGF binding to heparin or heparan sulfate in a membrane-binding setting (*9*) or in a biosensor-based assay (*17*). Two naturally occurring HGF isoforms NK1 (extending to K1) and NK2 (extending to K2) also bind c-Met and heparin and can function as agonists or antagonists of the full-length HGF (*5*, *10*, *14*, *18*). A heparin-binding constant similar to that for uncleaved HGF was found for NK2 by surface plasmon resonance techniques (*19*).

[†] Research was sponsored in part by the National Cancer Institute, DHHS, under contract with ABL and SAIC Frederick.

* Corresponding author. Phone: (301) 846-1218. Fax: (301) 846-6231. E-mail: rabyrd@ncifcrf.gov.

[‡] ABL-Basic Research Program.

[§] AIDS Vaccine Program.

[∥] Protein Expression Laboratory.

[⊥] Laboratory of Cellular and Molecular Biology.

[1] Abbreviations: HGF, hepatocyte growth factor; NMR, nuclear magnetic resonance; HS, heparan sulfate; SOS, sucrose octasulfate; FGF, fibroblast growth factor; NOE, nuclear Overhauser enhancement; FITC, fluorescein isothiocyanate; DTT, dithiothreitol.

10.1021/bi9908641 CCC: $18.00
Published on Web 00/00/0000 PAGE EST: 9.4

Following the report that the N domain retains the heparin-binding ability of full-length HGF (*10*), we determined the solution structure of this domain (*20*). Because interaction between heparin and protein is predominantly electrostatic (*21*), the structure immediately suggested a potential heparin-binding site which has a distinct cluster of positively charged residues. The recent crystal structure of the HGF isoform NK1 (*22*, *23*) reveals a nearly identical structure of the N domain within a "head-to-tail" NK1 dimer in the asymmetric unit. Although the dimer arrangement of NK1 suggests that heparin may have affinity to regions outside the N domain (*22*, *23*), mutational and biochemical data support the idea that the primary heparin-binding site resides in the N domain.

In this study, we conducted a series of heparin titration experiments that confirmed the previously proposed heparin-binding site in the N domain. The K_d of heparin−N domain binding in solution, estimated using nuclear magnetic resonance (NMR) and fluorescence techniques, is in the micromolar range, significantly lower than that found for a longer HGF fragment (NK2) or full-length HGF when assayed with membrane preparations or heparin attached to a solid phase. We examined the dynamic properties of the heparin-binding site by measuring the ^{15}N spin relaxation parameters of the N domain. These data indicate that the heparin-binding region undergoes conformational exchange on a microsecond to millisecond time scale in the absence of the ligand. The protein structure is stabilized upon heparin binding, as shown by increased resistance to disulfide bond reduction in the presence of heparin. We also conducted binding studies using a disaccharide heparin analogue, sucrose octasulfate (SOS). SOS has a structure and polyanionic character similar to those of the disaccharide repeating unit of heparin (*24*). Either in soluble form or as an insoluble aluminum salt, SOS has been used to treat stomach ulcers, and it appears to function by binding and stabilizing FGF (*24*−*26*). We observed that SOS binds to the HGF fragments N and NK1 at nearly the same region as that found for heparin binding. These results suggest a model of heparin-induced dimerization involving heparin binding to the primary sites and the N-terminal basic residues in the N domains of an HGF dimer.

MATERIALS AND METHODS

Sample Preparation. The N, K1, and NK1 fragments of HGF were expressed in *Escherichia coli*, refolded, and purified as previously described (*20*, *27*). Isotope-labeled proteins were expressed in M9 minimal media, containing either $^{15}NH_4Cl$ or both $^{15}NH_4Cl$ and ^{13}C-labeled glucose. All protein samples were dissolved in 50 mM sodium phosphate and 100 mM NaCl at pH ∼6.8 prior to the titration experiments. NMR data were collected at 30 °C on a Varian UnityPlus 500 or 600 MHz spectrometer equipped with Z-spec triple resonance probes with pulsed field gradients (Nalorac Corp.), except as otherwise stated.

*Heparin and SOS Titration*s. Porcine heparin, with an average molecular mass of ∼3 kDa (∼10−15 monosaccharide units) or 6 kDa, was purchased from Sigma. Purity of both heparin samples was checked by ^1H NMR spectroscopy at 70 °C (*28*, *29*) and found to contain <2% dermatan sulfate. SOS was purchased from Toronto Research Chemicals, Inc. In the NMR experiments, the titration was done by adding concentrated heparin or SOS solution (5−25 mM) to samples of the N domain or NK1 contained in 5 mm NMR tubes. At each ligand:protein ratio, a two-dimensional $^1H-^{15}N$ correlation spectrum or a one-dimensional ^1H spectrum was recorded, and changes in resonance position were examined.

Fluorescence Spectroscopy. Tyramine- and FITC-tagged heparin (*30*), with an average molecular mass of 4 kDa, was purchased from Sigma. The heparin was dissolved in water at a concentration of ∼5 μg/mL heparin. Fluorescence measurements were carried out in either a Spex Fluoromax-2 (Instruments SA) or a Shimadzu RF-5301PC (Shimadzu Scientific Instruments, Inc.) spectrofluorometer. The buffer was 50 mM sodium phosphate, pH 6.8, containing 100 mM NaCl. Tryptophan (Trp) emission spectra from the N and NK1 fragments of HGF were acquired in the ratio mode by exciting the sample at either 280 or 297 nm (2 nm bandwidth) and collecting the emission intensity between 290 and 550 nm (5 nm bandwidth) at 0.5 nm intervals for 0.3 s at each wavelength. Buffer subtraction was carried out to generate net spectra, which underwent zeroing at 540 nm. Spectral deconvolution of overall emission spectra was performed by subtraction of the spectrum obtained at 297 nm excitation (where Trp photoselection is maximal) normalized to the emission intensity at 380 nm (where Tyr does not contribute) from the overall emission spectrum taken with 280 nm excitation. Such a spectral manipulation yielded the net Tyr emission spectrum of the sample. Relative contributions of the Tyr and Trp populations to the overall emission were determined from the area under the spectra. Excitation spectra were acquired ratiometrically between 240 and 340 nm at 0.25 nm intervals with a 1 nm bandwidth and 1 s integration time, by monitoring the emission intensity at 360 nm. Excitation spectra were corrected for solvent background and lamp output intensity.

Fluorescein emission spectra from FITC-labeled heparin were acquired with 460 nm excitation and 2 nm bandwidth and measured between 480 and 700 nm at 0.5 nm intervals with a 5 nm bandwidth and 0.3 s integration time. Excitation spectra were obtained with identical settings, except that the emission was monitored at 550 nm and the excitation monochromator moved from 340 to 540 nm. Samples were placed in dual path length (0.2 × 1.0 cm) Suprasil quartz cuvettes (Uvonic Instruments, Inc.) in a thermostated holder at 25 °C.

^{15}N Relaxation. The longitudinal (T_1) and transverse (T_2) relaxation times of backbone amide ^{15}N nuclei and $^{15}N\{^1H\}$ nuclear Overhauser enhancements (NOEs) for the N domain were measured at proton frequencies of 500 and 600 MHz with the use of pulsed field gradients (*31*, *32*). Two-dimensional $^1H-^{15}N$ correlation spectra were collected with the following ^{15}N relaxation delays: 11.1, 55.5, 133.2, 188.7, 277.5, 444.0, 555.0, 721.5, 832.5, and 999.0 ms for T_1 and 15.5, 31.0, 46.5, 77.4, 92.9, 108.4, 123.9, 139.4, 154.9, and 185.9 ms for T_2. The recycle delays between the scans were 2 s for the T_1 and T_2 measurements. The relaxation time constants were extracted by fitting the intensity data of resolved amide NH cross-peaks to a single-exponential decay function of the delay time. Heteronuclear $^{15}N\{^1H\}$ NOEs were measured as the ratio of the peak intensities in the spectrum collected with ^1H saturation during a 3 s recycle delay and a spectrum without ^1H saturation.

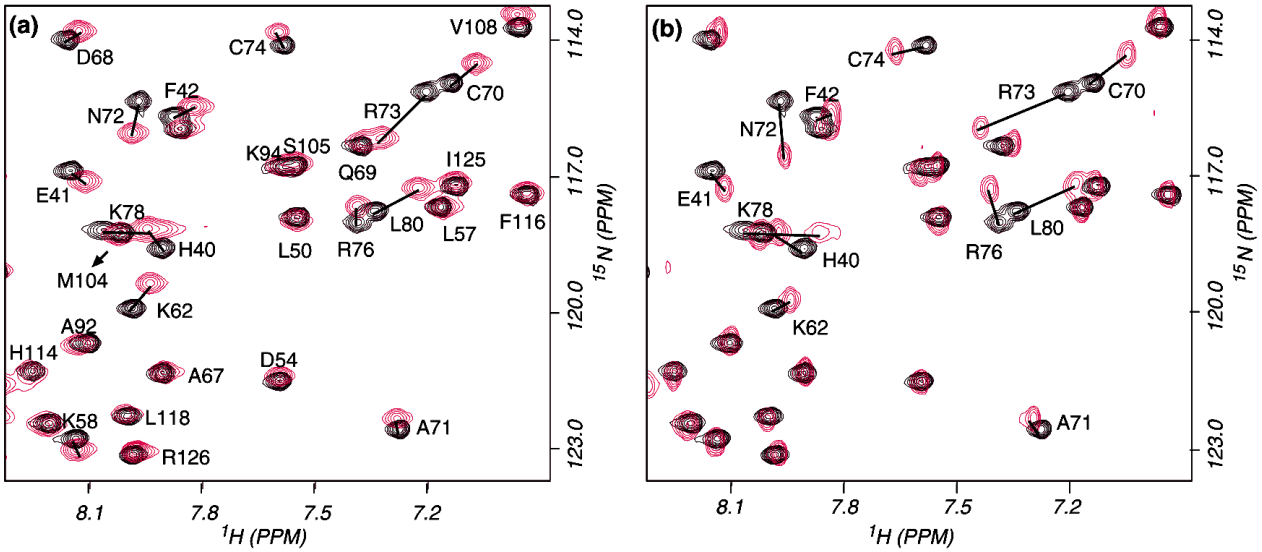

FIGURE 1: Overlay of portions of the ^{1}H−^{15}N correlation spectra of the N domain of HGF in the presence and absence of heparin (a) or SOS (b). The spectrum of the free protein is in black, and the spectrum in the presence of ligand is in red. The ratio of the ligand:protein concentration is 1:5 in (a) and 1:3 in (b).

The relaxation data were analyzed using the "model-free" approach (*33*) and the program ModelFree (*34*). For a nearly spherical molecule undergoing isotropic tumbling, the spectral density that governs the spin relaxation is described by an overall rotational correlation time (τ_m), a correlation time for internal motions (τ_e), and an order parameter (S^2):

$$J(\omega) = S^2\tau_m/[1 + (\omega\tau_m)^2] + (1.0 - S^2)\tau/[1 + (\omega\tau)^2]$$

where $\tau = \tau_m\tau_e/(\tau_m + \tau_e)$. A linear combination of $J(\omega)$ at different frequencies and with coefficients for dipolar coupling and chemical shift anisotropy gives rise to the relaxation rates R_1 ($1.0/T_1$) and R_2 ($1.0/T_2$) (*34*). An exchange term (R_{ex}) on a microsecond-to-millisecond time scale may contribute to R_2, which shortens T_2 and causes line broadening (*34*). To a first-order approximation, internal motions were ignored ($\tau_e = 0$), and T_1/T_2 (or R_2/R_1) ratios were fit to extract τ_m by minimizing the function:

$$E = \sum_{i,500,600}\{[(R_2/R_1)_{cal} - (R_2/R_1)_{exp}]/(R_2/R_1)_{exp}\}^2$$

where cal and exp denote calculated and experimental values, respectively, and the sum was obtained for selected residues and data at the two fields. Only residues with ^{15}N{^{1}H} NOE values larger than 0.65 and T_1/T_2 values within 1 standard deviation around the average were included in the fitting. With τ_m fixed at the best value calculated, the internal motion parameters S^2 and τ_e and the exchange rate R_{ex} were extracted by fitting R_1, R_2, and NOE for each residue, through the minimization of the function:

$$E = \sum_{i,500,600}\{[(R_{1,cal} - R_{1,exp})/R_{1,exp}]^2 + [(R_{2,cal} - R_{2,exp})/R_{2,exp}]^2 + [(NOE_{cal} - NOE_{exp})/NOE_{exp}]^2$$

RESULTS

Identification of the Heparin- and SOS-Binding Sites. The isolated N domain bound to heparin and SOS, as shown by the peak movements in the ^{1}H−^{15}N correlation spectrum with the addition of the ligands (Figure 1). The cross-peak displacements continued with each addition of ligands until saturation, indicating that the binding was on a fast-exchange time scale relative to the resonance frequency differences between the free and bound proteins. The residues that exhibited large changes in amide ^{1}H and ^{15}N resonances upon heparin binding were clustered in a surface formed by residues 60−80, which consist of a strand (β2), an α-helix, and a loop (Figures 2 and 3). The involvement of the loop in heparin binding was indicated by large displacements of the Arg76 and Leu80 amide resonances with the addition of heparin, although the amide resonances of several residues in the loop, including Lys78, have not been reliably assigned in both the free and bound proteins. SOS bound to HGF at nearly the same surface as heparin (Figure 3), but the region affected by binding appeared to be smaller and the most affected region was Arg73−Leu80. This was not surprising, since SOS is much smaller than a typical heparin molecule. Substantial resonance changes were also observed for residues 38−42 in the N-terminal, short helical region for both heparin and SOS binding. These changes may be due to contact of this region with the primary heparin-binding site in the structure or most likely the involvement of several basic residues in the N-terminal region of the N domain in ligand binding.

These observations confirmed the previous prediction of a heparin-binding site based on surface charge distribution (*20*). Heparin binding primarily involves Lys60, Lys62, and particularly Arg73 (Figure 3). These residues showed large changes in chemical shift upon ligand binding. Interestingly, a sulfate ion was coordinated by these residues in one form of the NK1 crystal structure (*23*). Basic residue clusters that are remote from this binding center did not seem to have significant interactions. In particular, several basic residues in a tight turn (Lys91/Arg93/Lys94) had only small changes in their amide chemical shifts. In SOS binding, the most significant changes in chemical shift were observed around Arg73 and in the following loop region (Asn77−Leu80), and moderate changes were observed in the N-terminal region and strand β2. Several new peaks in the ^{1}H−^{15}N correlation

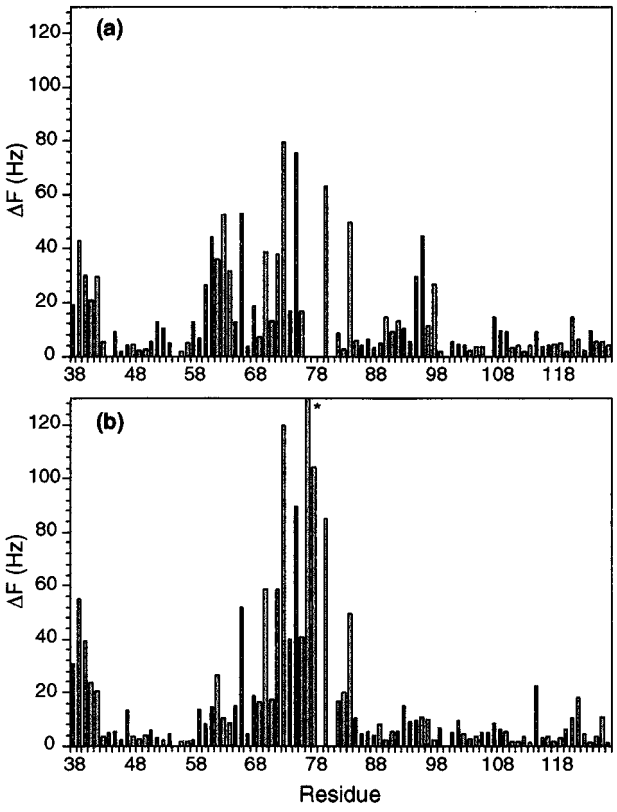

FIGURE 2: Amide resonance frequency changes of the N domain of HGF upon binding to heparin (a) and SOS (b). The frequency change represents the total displacement of the amide cross-peak in the $^{1}H-^{15}N$ correlation spectrum with the addition of the ligand, $(\Delta H + \Delta N)^{1/2}$, measured in hertz at the proton field of 500 MHz. The ratio of the ligand:protein concentration is 1:5 in (a) and 1:3 in (b). The maximum change in (b), indicated by an asterisk, is 206 Hz for Asn77 and is truncated at the top for better scaling of the data.

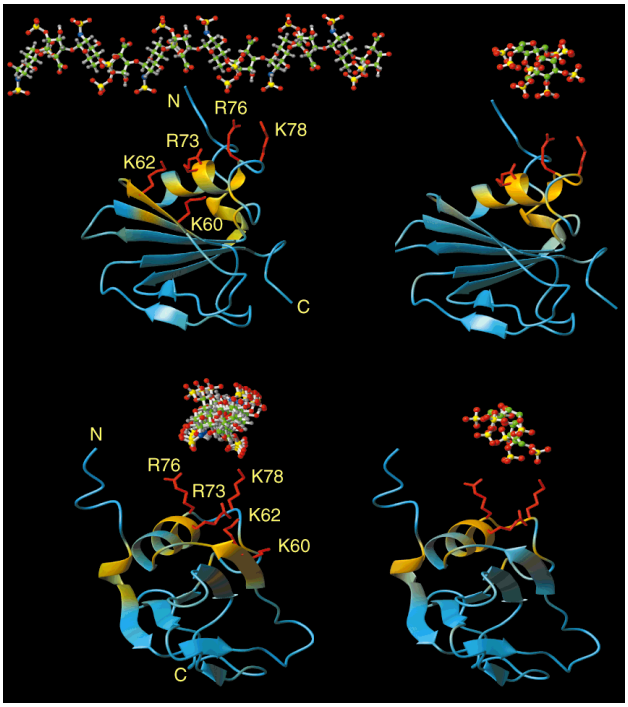

FIGURE 3: Schematic representation of the resonance changes for the N domain of HGF upon binding to heparin (left) or SOS (right). The bottom two figures result from a 90° rotation of the top figures. The color scheme corresponds to an increasing change in resonance frequency, from cyan to gold, with the addition of the ligand. The amplitude of the resonance frequency change is taken from Figure 2. A 12-residue heparin (*42*) or SOS (*25*) is shown above the protein structure, with sulfur atoms in yellow, oxygen atoms in red, and carbon atoms in green. The orientation of the ligand relative to the protein is not known. The heavy-atom side chains of the basic residues situated within the region of ligand binding are shown in red. The N-terminus of the protein is located in the upper left corner of the structure. The plot was generated with the program MOLMOL (*45*).

spectrum of the SOS-bound protein came from the loop region and the N-terminal residues, due to the tightening and reduced mobility of the structure upon ligand binding (H. Zhou and R. A. Byrd, manuscript in preparation). It is interesting to note that the helical and the loop regions also contain several polar residues which are aligned linearly along one surface of the helix at the edge of the heparin-binding site. Among these polar residues, Asn72, Thr75, and Asn77 exhibited large resonance changes upon ligand binding. The polar side chains of these residues may form hydrogen bonds with heparin, as seen in several heparin−FGF complex structures (*13*, *35*).

In addition to the significant resonance changes mentioned above, several residues around Cys96 also showed large displacements of amide resonances in the presence of heparin. Cys96 resides in strand β4, which aligns with strand β2 through hydrogen bonds. The changes around Cys96 are probably due to structural rearrangement at the binding surface that is transduced by the disulfide linkage between Cys96 and Cys70. Smaller resonance changes occurred in the same region in SOS binding, indicating that strand β2 was not extensively involved in SOS binding. This finding is consistent with the primary binding site for SOS being localized within the α-helix and the following loop region.

Heparin and SOS Binding of NK1. Similar NMR titration experiments were conducted for NK1. Heparin and SOS binding to NK1 was substantially different from binding to the N domain. Heparin caused precipitation of NK1, although an excess of heparin slightly decreased the precipitation. With the addition of heparin, the amide peaks remained at the same position but dropped in intensity and eventually all peaks, except for a few intense peaks, disappeared, suggesting the formation of a large heparin−NK1 complex. The remaining intense peaks were mostly from side chain amide groups and from a highly flexible region of the protein. The precipitation prevented us from examining the resonance changes of NK1 upon binding to heparin.

SOS aggregated NK1 to a lesser extent than heparin. A small amount of precipitation was observed after SOS was added to the protein sample, but $^{1}H-^{15}N$ resonances, from protein molecules in solution, could still be detected (Figure 4). The exchange between free and bound proteins was fast relative to the resonance frequency differences between free and bound conformations, as shown by the presence of a single set of cross-peaks for the residues involved in binding and the continuous movement of the peaks with the addition of SOS. The residues that have large changes in chemical shifts upon SOS binding can be assigned almost entirely to the N domain. The direction and amplitude of the peak movement closely resemble those in the N domain−SOS binding, indicating essentially the same ligand binding sites and similar structural changes in the N domain and NK1. Although K1 did not bind to a heparin−Sepharose column

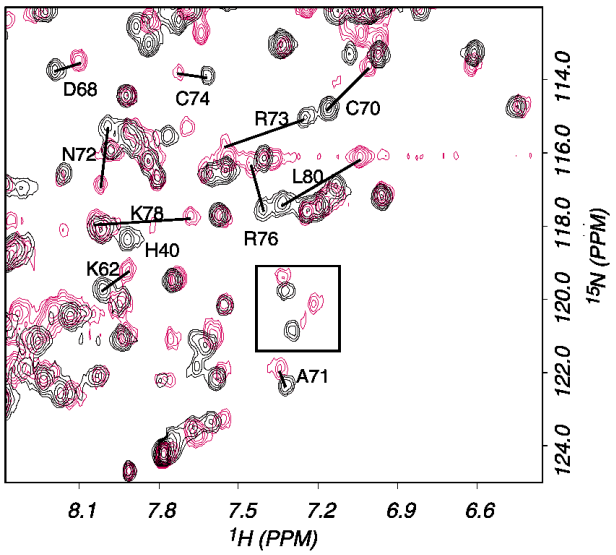

FIGURE 4: Overlay of portions of the ^{1}H−^{15}N correlation spectra of NK1 in the presence (red) or absence (black) of SOS. The straight lines indicate the change of amide peak positions when an excess of SOS was added to the protein sample. The peaks inside the box are from the K1 domain.

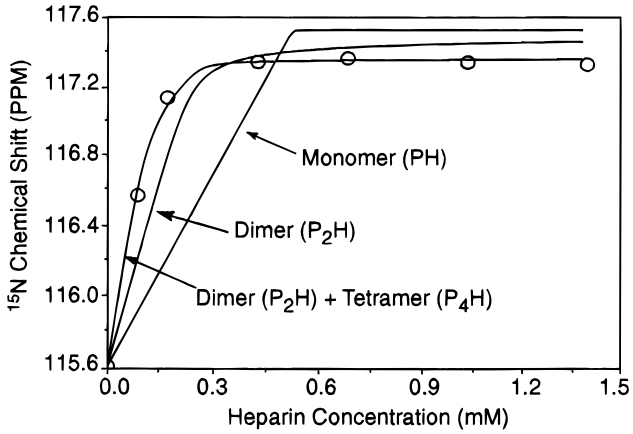

FIGURE 5: Binding of multiple protein molecules by a single heparin. The chemical shift of Arg73 amide ^{15}N (open circles) in the isolated N domain of HGF is shown as a function of the total heparin concentration. The solid line is the theoretical best fit of the data, using a model assuming a heparin:protein stoichiometry of 1:1, 1:2, and (1:2 + 1:4) of the complex. The following equilibria are assumed: P + H ↔ PH for the 1:1 complex; 2P + H ↔ P_2H for the 1:2 complex; 2P + H ↔ P_2H, 2P + P_2H ↔ P_4H for the (1:2 + 1:4) complex. The equilibrium equations can be found, for example, in ref *46*. The measured chemical shift is taken as the fractional average of those in the free and bound protein under fast-exchange condition. We also assume that there is only a single ligand-binding site in the protein, with a single chemical shift value for the bound state. A separate dissociation constant is assumed for each equilibrium, and the total differences between the measured and calculated chemical shifts were minimized in a grid-search manner by varying the apparent dissociation constants and the chemical shifts of the bound state. Due to the large number of unknown parameters and the small dissociation constant relative to the protein and ligand concentrations used, this analysis is only used to show the presence of ligand-induced oligomerization and should be viewed qualitatively.

in a previous study (*10*), we observed that several amide NH resonances from the K1 domain in NK1 moved with the addition of SOS. Addition of a 10-fold excess of SOS to a K1 sample also caused peak movements for these amide resonances, indicating that SOS weakly binds to the isolated K1 domain and to the K1 domain within NK1.

Despite the slight aggregation of NK1 with SOS, the observed NK1 resonances were not significantly broadened relative to the peaks in the free protein (Figure 4), indicating that at least one mode of SOS binding to NK1 does not involve significant formation of dimers or oligomers. The formation of NK1 dimer or oligomers would increase the molecular mass of the complex to at least 44 kDa and would cause significant line broadening or even resonance disappearance. Because SOS is much shorter than a typical heparin molecule, the data from NK1−SOS binding does not rule out that heparin is able to oligomerize NK1 and induce a more stable, high-molecular-weight complex with NK1. Heparin-induced NK1 oligomerization was indicated by the aggregation of NK1 in the presence of heparin. Binding of heparin to the interdomain interface within an NK1 or NK2 dimer has also been suggested on the basis of the recent crystal structures of NK1 (*22*, *23*). Such a binding mode requires the ligand to be long enough to bridge two or more domains within or between the monomers.

Heparin-Induced Oligomerization of the N Domain. In the case of both heparin and SOS binding, the resonance peak positions in the isolated N domain exhibited a clear dependence on ligand concentration, indicating a chemical shift averaging effect due to an apparent fast exchange between free and bound conformations. The binding curves could not be fit with a simple two-site fast-exchange model, P + H ↔ PH, which involves only monomeric protein (P) and heparin (H) with a single binding site on each molecule (Figure 5). The fast transition in chemical shift from the free state to the bound state suggests ligand-induced oligomerization of the protein or multiple, cooperative binding sites for heparin. A model which included a 1:2 heparin−protein complex in the bound state significantly improved the fit and including a 1:4 complex further improved the fit (Figure 5). The formation of a complex involving two or more protein molecules in the presence of heparin was also indicated by severe line broadening of the amide resonances in the presence of an excess of ligand.

Structural Flexibility of the N Domain. To determine whether the heparin- and SOS-binding region is dynamically different from the remainder of the free protein, we collected and analyzed the ^{15}N relaxation data at field strengths corresponding to ^{1}H frequencies of 500 and 600 MHz for the N domain (Figure 6). Also of interest was the dynamics of the two extended loop regions encompassed by residues 47−59 and 100−116. By simultaneously fitting the T_1/T_2 ratios at the two fields, we obtained an overall rotational correlation time of 6.5 ns, which is reasonable for a nearly spherical, monomeric protein of 11 kDa. Residues 72−85, which include the C-terminal half of the α-helix and the loop region (Asn77−Pro81), exhibited significantly reduced T_2 values. A chemical shift exchange term (R_{ex}) was added to the fitting to account for this T_2 reduction, leading to R_{ex} values larger than 1 Hz for most residues in this region. Residues 75 and 76 had the shortest T_2 values, which led to R_{ex} values of ∼5 Hz. Several residues in the loop region immediately after the α-helix were not observed in the ^{1}H−^{15}N spectrum. These results indicate that a large portion of the heparin-binding region and particularly the loop region are involved in motions on a microsecond-to-millisecond time scale. The two extended loop regions showed slightly

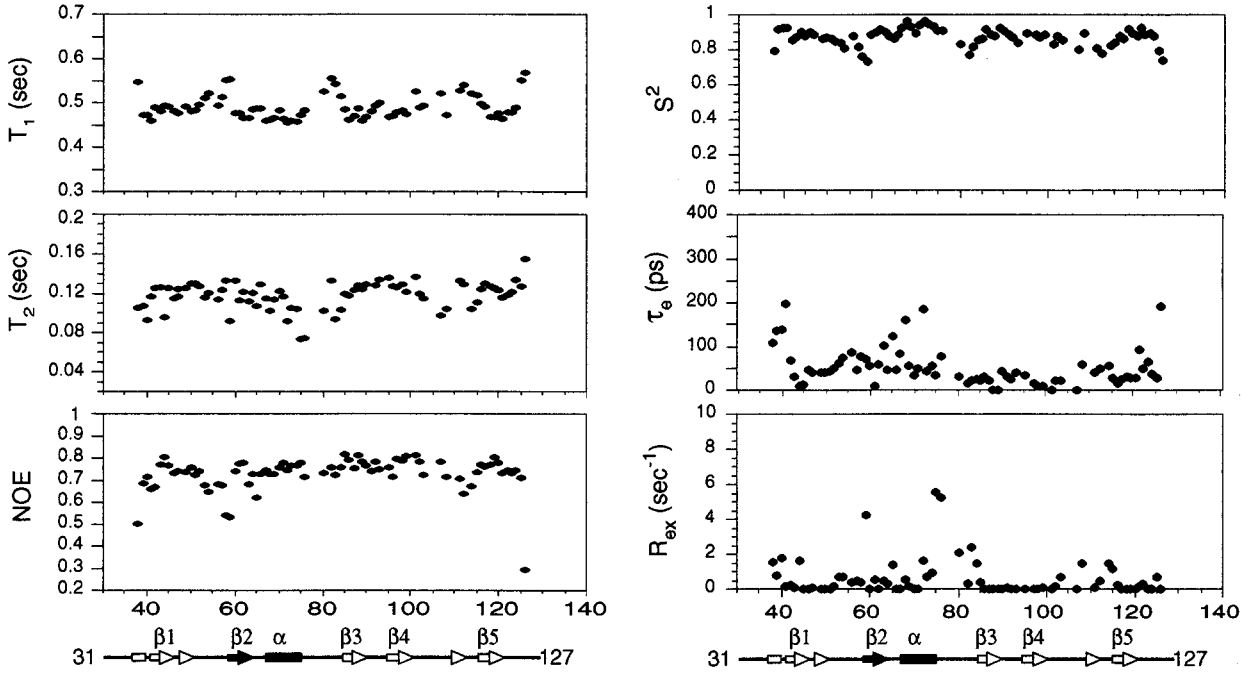

FIGURE 6: ^{15}N relaxation data of the N domain of HGF. The left panels show the longitudinal (T_1) and transverse (T_2) relaxation times and the ^{15}N−^{1}H NOE factors at the ^{1}H field of 500 MHz. The right panels show the calculated order parameter (S^2), correlation time of internal motions (τ_e), and exchange rate (R_{ex}). The secondary structure is shown at the bottom of the left and right panels. Helices are indicated by rectangles and β-strands by arrows. The region that contains the primary heparin-binding site is indicated by the solid rectangle and arrow.

reduced order parameters, especially in the regions of residues 54−59 and 107−115, but overall these extended loops exhibited a high degree of rigidity. The N-terminal seven residues were not observed in the NMR spectrum. Their absence apparently resulted from line-broadening effects from high levels of mobility on a microsecond-to-millisecond time scale, as indicated by the increasing trend of R_{ex} and τ_e toward the N-terminus.

Increased Protein Stability against Disulfide Bond Reduction in the Presence of Heparin. Because heparin and SOS stabilize the structure of FGF (*13*, *24*−*26*), we investigated this effect for HGF by observing the increased stability of HGF against chemical reduction in the presence of heparin. The N domain contains two disulfide bridges (Cys70−Cys96 and Cys74−Cys84). In the absence of heparin, a 10-fold molar excess of DTT denatured the protein in approximately 24 h (Figure 7), presumably by disrupting the "hairpin loop" structure (*20*) linked by the disulfide bridges. In the presence of heparin, however, the protein remained folded for more than 96 h in the presence of DTT. The solution structure of the N domain (*20*) reveals that the Cys70−Cys96 bond is entirely buried in the core of the protein, whereas the Cys74−Cys84 bond is covered by the flexible loop (Asn77−Pro81). The results of the chemical reduction experiment support the notion that the loop region formed by residues 77−81 is flexible in the free protein and is able to open up and allow the reducing agent access to at least one of the disulfide bonds. The data indicate that the loop region became more rigid when heparin was bound to the protein and ligand binding prevented DTT from coming in contact with the disulfide bonds. Because the two basic residues in the loop region, Arg76 and Lys78, lie near the edge of the heparin-binding surface, they probably play a facilitating role in binding heparin.

Measurement of the K_d of Heparin−N Domain Binding by Fluorescence Spectroscopy. To study heparin−N domain interaction at a concentration comparable to the K_d, we conducted a series of titration experiments using fluorescence techniques. The emission spectrum of the N domain was clearly the composite of multiple bands (data not shown). The resolved Trp band was notably red-shifted, with an emission maximum (354 nm) typical of indole side chains that are exposed to the solvent environment. The Trp band was also relatively broad (5800 cm^{-1}), with a line width that was much larger than that measured from the excitation spectrum (4850 cm^{-1}) of the N domain. Such a large line width for the photoselected Trp emission cannot be explained by a Tyr to Trp energy transfer process at the singlet level. Rather, it must reflect the inhomogeneous microenvironment of the emitting fluorophore, stemming from sampling of multiple locations of different polarity by the sole Trp fluorophore in the N domain. The N domain structure shows that Trp98 is partially buried and surrounded by the positively charged side chains of Lys and Arg. This unusual environment for a hydrophobic indole moiety is in good agreement with the low fluorescence emission of this particular residue.

The intrinsic fluorescence emission of the N domain did not change significantly upon addition of heparin or SOS sodium salt. Association of heparin with the N domain did apparently occur, since addition of heparin to the N domain complexed with fluorescein-labeled heparin displaced the latter (see below). Addition of heparin to NK1 resulted in precipitation, precluding further study of the interaction. To quantify the binding of heparin to the N domain, we used a commercial preparation of FITC-labeled heparin (*28*) (average molecular mass ∼4 kDa) in the binding assays. Spectrofluorometric characterization of the labeled material showed excitation and emission maxima at 492 and 514 nm, respectively, which are typical of the fluorescein moiety. Addition of saturating amounts of the N domain to FITC−heparin resulted in a 44% (±1%) reduction in the fluorescein emission intensity. Analysis of such equilibrium binding

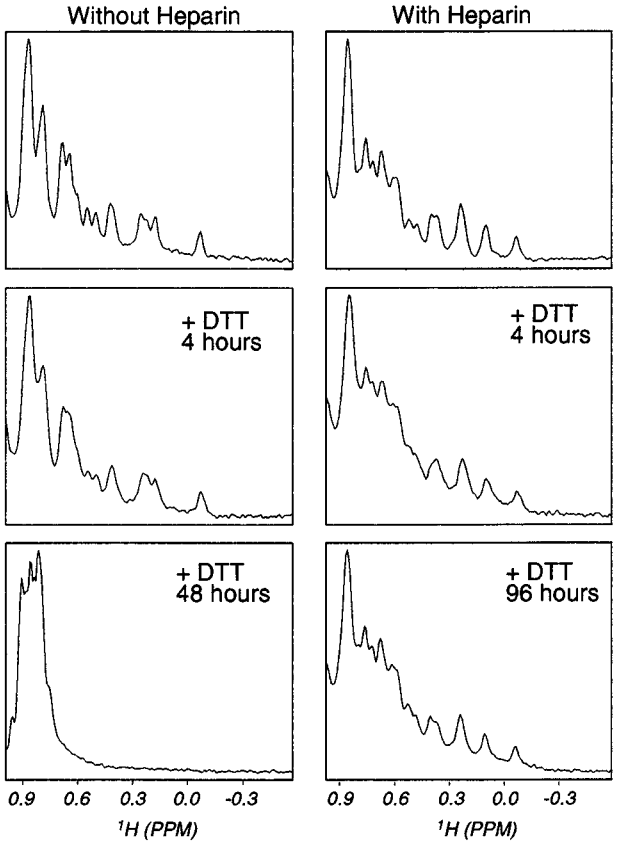

FIGURE 7: Increased stability of the protein against disulfide bond reduction in the presence of heparin. A 10-fold excess of DTT was added to the isolated N domain samples at the concentration of 50 μM in the absence (left) or presence (right) of 1 mM heparin. One-dimensional ^{1}H NMR spectra were collected after the specified time indicated inside each panel. Unfolding of the protein in the absence of heparin is indicated by the collapse of the proton resonance toward random-coil values and was detected within approximately 24 h after the addition of DTT. The spectrum remained unchanged for more than 96 h in the presence of heparin.

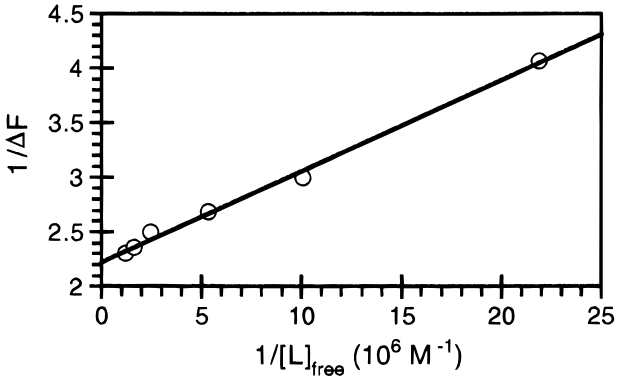

FIGURE 8: Double-reciprocal plot for the interaction of the N domain of HGF with FITC-labeled heparin. The reciprocal of the free NK1 concentration ($1/[L]_{free}$) was plotted vs the reciprocal of the fractional, normalized change in fluorescence emission intensity ($1/\Delta F$). Points were fitted by linear regression, which yielded a rectilinear trace that indicates the limiting quenching at saturation and the binding affinity of the interaction. Experimental conditions are reported in Materials and Methods.

isotherms according to a Langmuir model (*36*), which describes independent binding to isolated sites, resulted in rectilinear traces ($R^2 > 0.996$) in double-reciprocal plots (Figure 8) of $1/\Delta F$ vs $1/[\text{ligand}]_{free}$, from which we derived a dissociation constant of 0.17 ($\pm$0.02) μM and a stoichiometry of 0.82 ($\pm$0.25):1 for the interaction of FITC−heparin with the N domain (duplicate determinations). Any possible effect of the hydrophobic fluorescein label on the interaction with the N domain was investigated in competition experiments with unlabeled heparin.

Displacement of FITC−heparin from the N domain was attempted by addition of unlabeled heparin (average molecular mass ~3 kDa) to a preformed complex. Although displacement was observed and rapid reequilibrium was achieved under our experimental conditions, a significant excess of unlabeled heparin was required for a 50% displacement, suggesting that the interaction of the N domain with FITC−heparin was about 1 order of magnitude stronger than with the unlabeled material. Stepwise titrations of the N domain into a mixture of heparin and FITC−heparin in a 1:1 or 9:1 molar ratio confirmed this finding and showed a 7-fold higher affinity of the N domain for FITC−heparin, relative to unlabeled heparin. Thus, the binding affinity of HGF−N for heparin was determined as 1−2 μM.

DISCUSSION

Primary Heparin-Binding Site. We have identified the primary heparin-binding site in the N domain of HGF through heparin and SOS titration experiments. In the well-characterized FGF system, studies of heparin−FGF binding have shown the extreme complexity of the heparin−protein interactions that involve multiple binding sites in the protein, the formation of protein dimers and tetramers in addition to the monomeric species, and several spatial configurations of the oligomer and heparin (*11*). Given the multidomain organization of HGF and the possible existence of additional binding sites outside the primary site in the N domain, the HGF−heparin interaction is likely to be even more complex. This study focuses on the primary heparin-binding site in the N domain and represents the first step toward understanding the various modes of HGF−heparin interaction.

The primary heparin-binding site identified in this paper consists of Arg73, Lys60, and Lys62, with additional contributions from Arg76 and Lys78. This finding is consistent with the significant reduction in heparin affinity when Arg73 or Lys78 was substituted with alanine in a naturally occurring HGF variant, dHGF (*37*), and the nearly complete loss of heparin affinity for the group mutation R73E/R76E/K78E of HGF (*19*). On the other hand, alanine subsitution of Lys91, Arg93, and Lys94 has almost no effect on heparin affinity (*10, 37*), consistent with the small chemical shift changes observed when heparin was added. Therefore, these residues are not part of the primary heparin-binding site.

Involvement of the N-Terminal Basic Residues in Heparin Binding. There is published evidence that indicates the N-terminal basic residues are directly involved in heparin binding. Alanine substitution of the four basic residues (RKRR) near the N-terminus resulted in a 32% reduction in heparin-binding ability of full-length dHGF (*37*). Because this region is flexible in the absence of ligand, mutations in this region are unlikely to affect the native fold of the protein. Consequently, the effects observed in the alanine substitution studies probably reflect the heparin affinity for this region. Isolation of heparin-binding fragment peptides through limited protease digestion also indicated an important role

of the N-terminal region in heparin binding (*38*). In our studies, we observed significant resonance frequency changes and reduction of flexibility in the N-terminal region upon ligand binding, consistent with direct contact of this region with the ligand. However, our data do not suggest that these basic residues form an independent binding site with an affinity comparable with that of the primary binding site. If both regions bind heparin independently and with nearly equal affinity, the saturation of binding sites in the protein would be much slower than we observed. Together, the published mutation data and the data presented here suggest that heparin binding involves additive contributions from three regions: the primary binding site formed by Arg73, Lys60, and Lys62; the N-terminal basic residues; and the flexible loop region (Asn77−Leu80).

Heparin Affinity of the Isolated N Domain. In our titration experiments, which were monitored by both NMR and fluorescence and covered a protein concentration range from upper nanomolar to millimolar, we observed a micromolar K_d for the isolated N domain. This dissociation constant is significantly higher than the nanomolar K_d observed for the interaction of the full-length protein or NK2 with surface-immobilized ligands (*9*, *17*, *19*). Increasing the pH from 6.8 to 7.4 or the salt concentration from 100 to 200 mM in our NMR experiments did not have a significant effect on the binding (data not shown). This discrepancy in apparent binding affinity can be attributed, in part, to the differences of binding to surface-associated heparin-like molecules, subject to two-dimensional diffusion, versus binding in solution, subject to three-dimensional diffusion (*12*, *39*). It may also result from differences of the oligomerization ability between HGF fragments of different lengths (vide infra) and/or the existence of additional binding sites outside the N domain. Earlier experiments also implicated a role for the K2 domain in heparin binding, evidenced by the loss of heparin affinity when K2 was deleted from HGF (*40*). A weak association of K1 with SOS was detected for both the NK1 and K1 fragments in our NMR experiments, and this finding is consistent with the fact that a HEPES molecule is bound to K1 in one crystal structure of NK1 (*23*). The weakness of this interaction implies that the binding is nonspecific.

It is worth noting that fluorometric titrations are consistent with a 1:1 complex between the N domain and heparin, whereas a 3 (±1):1 stoichiometry was inferred from NMR titration (Figure 4). This difference is probably not due to interference from the fluorescent label, since (1) the label is attached to the nonreducing end of heparin and leaves the antithrombin III binding sites unmodified and (2) the label does not perturb the anticoagulant activity of heparin (*30*). The larger size of FITC−heparin (~4 kDa) relative to the unlabeled heparin used (~3 kDa) also makes the effect of the fluorescent label less likely. This difference in the estimated stoichiometry probably results from multiple binding sites in heparin with different affinities to the protein, which is very plausible given the nearly symmetrical, helix-like structure of free (*41*, *42*) and bound (*13*, *35*) heparin. It is conceivable that, if binding sites with dissimilar affinity are present in heparin, the higher concentration regime (by 2−3 orders of magnitude) of the NMR experiments could result in their occupancy with the N domain. Analysis of NMR titrations yielded an approximate apparent binding constant of ~15 μM, which lends support to this hypothesis.

Heparin Binding to the N Domains in an NK1 Dimer. No evidence from our NMR experiments suggests that the N domain and NK1 have significant dimer or oligomer content in the absence of heparin, although a small amount of dimer was previously observed by cross-linking experiments (*10*, *14*). In the presence of heparin or other sulfated oligosaccharides, significant amounts of dimer or oligomer were observed for both FGF (*11*, *12*, *43*) and HGF (*10*, *14*, *15*, *22*). On the basis of the NK1 crystal structure, several possibilities of heparin-induced HGF dimerization have been proposed, although the physiological significance of the dimer structure is unknown. These possibilities include binding of a single heparin molecule to the primary site in one protomer and Lys91/Arg93 of the N domain in the other protomer (*22*) and binding of a long heparin molecule to an extended, positively charged groove at the interface between the N domain and both kringle domains in an NK2 monomer (*23*). The latter arrangement is unique since the proposed binding site lies outside the primary binding site.

Here we propose another possibility that takes into account heparin binding to the primary sites and the N-terminal residues in an NK1 dimer. The crystal structure of NK1 shows that the N-terminal segments from the two subunits in the dimer are positioned next to each other at the center of the dimer, with the two primary heparin-binding sites situated nearby (Figure 9). A heparin molecule with 10 or more saccharide residues is long enough to bridge the two primary binding sites and establish additional favorable electrostatic interactions with the N-terminal protein segments in the middle. Any steric interference of the N-terminal residues with heparin could be compensated by the flexibility of both this segment and heparin. The length of the heparin-binding region in this model is consistent with reports of the minimal size of the oligosaccharide (>10−12 residues) required for optimal binding to HGF (*44*). Our model proposes additive interactions of a single heparin molecule with four regions in the protein dimer: the two major-binding sites at either end of the binding region and the two N-terminal segments in the middle (Figure 9). The observed flexibility of the N-terminal segment, which is reduced upon ligand binding, permits an adaptive recognition to the heterogeneous glycosaminoglycans. Although a shorter oligosaccharide could bind to each individual site, it would not stabilize the dimer as well as a longer heparin molecule (*15*). This suggestion is supported by the finding that the minimal oligosaccharide that has significant affinity for HGF or is able to enhance HGF-dependent mitogenesis is a hexasaccharide (*15*, *44*).

Besides the supporting evidence indicated above, our model is also consistent with the fact that receptor- and heparin-binding regions in HGF are for the most part distinct (*10*, *19*). It has been shown that K1 retains most of the receptor-binding determinants (*6*, *7*) while the N domain retains most of the heparin-binding determinants (*10*). Indeed, most of the residues in K1 (Glu159, Ser161, Glu195, and Arg197) that were found to be significant in receptor binding (*7*) are located on the opposite side of the NK1 molecule from the heparin-binding region, as proposed in our model. This NK1−heparin-binding model maximizes the interaction between a single heparin molecule and the N domains in a NK1 dimer and minimizes binding of heparin to other

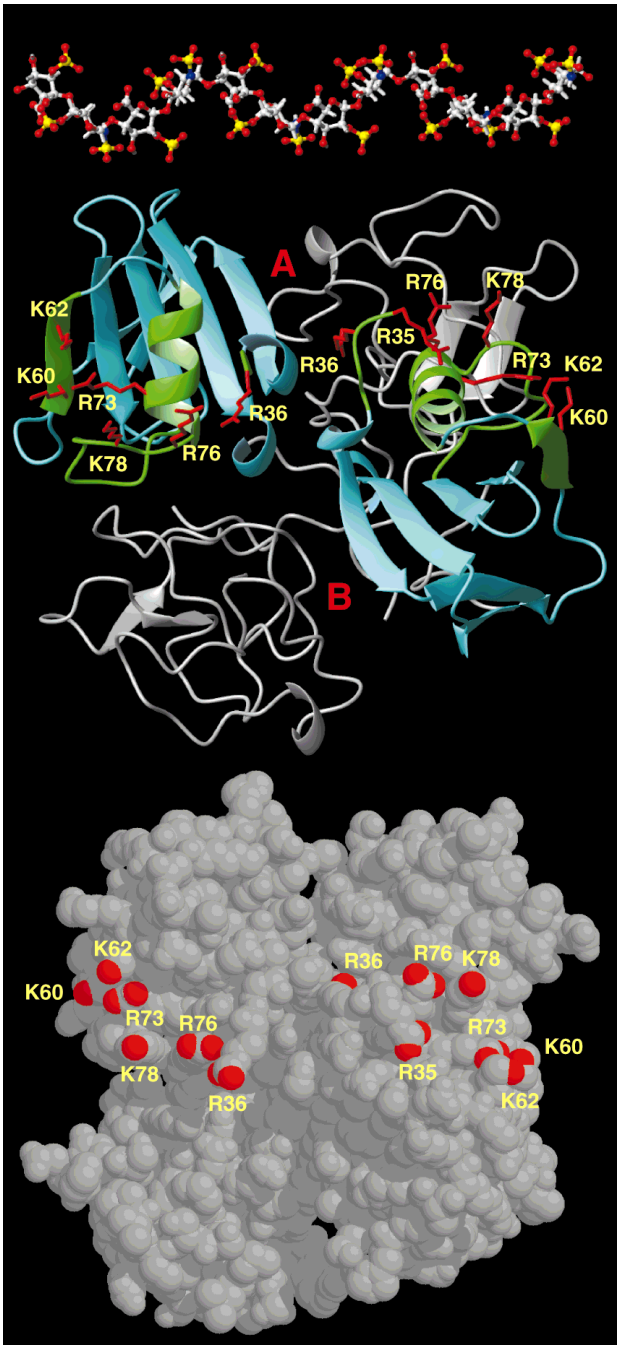

FIGURE 9: A heparin-binding model for an NK1 dimer. The K1 domains are shown in gray and the N domains are shown in cyan and green in the ribbon diagram (middle). The green region is involved in heparin binding in the isolated N domain, as indicated by the resonance changes upon binding. The side chains of the basic residues that form the primary binding site are shown in red. The N-terminal region, starting at residue 35 in one protomer and residue 36 in the other, is located at the center of the structure. A 12-residue heparin molecule (*42*) is shown above the NK1 structure. Sulfur, oxygen, and nitrogen atoms are in yellow, red, and blue, respectively. The primary binding sites and the N-terminal basic regions in the NK1 dimer form a nearly linear stretch of positive charges, which may interact with high affinity with heparin of 10 residues or longer. A space-filling model of the NK1 dimer structure is shown at the bottom, with nitrogen atoms of the arginine and lysine side chains in the binding site in red. The model is based on the NK1 dimer structure of ref *23* (PDB access code: 1BHT).

domains in HGF. This observation suggests that heparin does not significantly alter the structure of the receptor-binding sites, and its role is to bring two or more HGF and, in turn, receptor molecules together in a biologically active, oligomerized state. This model may assist in determining whether the dimer arrangement in the NK1 crystal structure has physiological significance.

SUPPORTING INFORMATION AVAILABLE

Two tables containing the T_1, T_2, and NOE values from the ^{15}N relaxation measurement and the extracted dynamics parameters for the N domain of HGF. This information is available free of charge via the Internet at http://pubs.acs.org.

REFERENCES

1. Miyazawa, K., Tsubouchi, H., Naka, D., Takahashi, K., Okigaki, M., Arakaki, N., Nakayama, H., Hirono, S., Sakiyama, O., and Takahashi, K. (1989) *Biochem. Biophys. Res. Commun. 163*, 967−973.
2. Nakamura, T., Nishizawa, T., Hagiya, M., Seki, T., Shimonishi, M., Sugimura, A., Tashiro, K., and Shimizu, S. (1989) *Nature 342*, 440−443.
3. Matsumoto, K., and Nakamura, T. (1996) *J. Biochem. 119*, 591−600.
4. Matsumoto, K., and Nakamura, T. (1997) *Ciba Found. Symp. 212*, 198−211.
5. Cioce, V., Csaky, K. G., Chan, A. M. L., Bottaro, D. P., Taylor, W. G., Jensen, R., Aaronson, S. A., and Rubin, J. S. (1996) *J. Biol. Chem. 271*, 13110−13115.
6. Lokker, N. A., Mark, M. R., Luis, E. A., Bennett, G. L., Robbins, K. A., Baker, J. B., and Godowski, P. J. (1992) *EMBO J. 11*, 2503−2510.
7. Lokker, N. A., Presta, L. G., and Godowski, P. J. (1994) *Protein Eng. 7*, 895−903.
8. Zarnegar, Z., DeFrances, M. C., Oliver, L., and Michalopoulos, G. (1990) *Biochem. Biophys. Res. Commun. 173*, 1179−1185.
9. Arakaki, N., Hirono, S., Ishii, T., Kimoto, M., Kawakami, S., Nakayama, H., Tsubouchi, H., Hishida, T., and Daikuhara, Y. (1992) *J. Biol. Chem. 267*, 7101−7107.
10. Sakata, H., Stahl, S. J., Taylor, W. G., Rosenberg, J. M., Sakaguchi, K., Wingfield, P. T., and Rubin, J. S. (1997) *J. Biol. Chem. 272*, 9457−9463.
11. Waksman, G., and Herr, A. B. (1998) *Nat. Struct. Biol. 5*, 527−530.
12. Herr, A. B., Ornitz, D. M., Sasisekharan, R., Venkataraman, G., and Waksman, G. (1997) *J. Biol. Chem. 272*, 16382−16389.
13. DiGabriele, A. D., Lax, I., Chen, D. I., Svahn, C. M., Jaye, M., Schlessinger, J., and Hendrickson, W. A. (1998) *Nature 393*, 812−817.
14. Schwall, R. H., Chang, L. Y., Godowski, P. J., Kahn, D. W., Hillan, K. J., Bauer, K. D., and Zioncheck, T. F. (1996) *J. Cell Biol. 133*, 709−718.
15. Zioncheck, T. F., Richardson, L., Liu, J., Chang, L., King, K. L., Bennet, G. L., Fugedi, P., Chamow, S. M., Schwall, R. H., and Stack, R. J. (1995) *J. Biol. Chem. 270*, 16871−16878.
16. Rubin, J. S., Chan, A. M.-L., Bottaro, D. P., Burgess, W. H., Taylor, W. G., Cech, A. C., Hirshfield, D. W., Wong, J., Miki, T., Finch, P., and Aaronson, S. A. (1991) *Proc. Natl. Acad. Sci. U.S.A. 88*, 415−419.
17. Rahmoune, H., Rudland, P. S., Gallagher, J. T., and Fernig, D. G. (1998) *Biochemistry 37*, 6003−6008.
18. Chan, A. M., Rubin, J. S., Bottaro, D. P., Hirschfield, D. W., Chedid, M., and Aaronson, S. A. (1991) *Science 254*, 1382−1385.
19. Hartmann, G., Prospero, T., Brinkmann, V., Ozcelik, Ö., Winter, G., Hepple, J., Batley, S., Bladt, F., Sachs, S., Birchmeier, C., Birchmeier, W., and Gherardi, E. (1997) *Curr. Biol. 8*, 125−134.
20. Zhou, H., Mazzulla, M. J., Stahl, S. J., Wingfield, P. T., Rubin, J. S., Bottaro, D. P., and Byrd, R. A. (1998) *Structure 6*, 109−116.
21. Jackson, R. L., Busch, S. J., and Cardin, A. D. (1991) *Physiol. Rev. 71*, 481−539.

22. Chirgadze, D. Y., Hepple, J. P., Zhou, H., Byrd, R. A., Blundell, T. L., and Gherardi, E. (1999) *Nat. Struct. Biol. 6*, 72−79.
23. Ultsch, M., Lokker, N. A., Godowski, P. J., and de Vos, A. M. (1998) *Structure 6*, 1383−1393.
24. Folkman, J., Szabo, S., Stovroff, M., McNeil, P., Li, W., and Shing, Y. (1991) *Ann. Surg. 214*, 414−425.
25. Zhu, X., Hsu, B. T., and Rees, D. C. (1993) *Structure 1*, 27−34.
26. Volkin, D. B., Verticelli, A. M., Marfia, K. E., Burke, C. J., Mach, H., and Middaugh, C. R. (1993) *Biochim. Biophys. Acta 1203*, 18−26.
27. Stahl, S. J., Wingfield, P. T., Kaufman, J. D., Pannell, L. K., Cioce, V., Sakata, H., Taylor, W. G., Rubin, J. S., and Bottaro, D. P. (1997) *Biochem. J. 326*, 763−772.
28. Holme, K. R., and Perlin, A. S. (1989) *Carbohydr. Res. 186*, 301−312.
29. Neville, G. A., Mori, F., Holme, K. R., and Perlin, A. S. (1989) *J. Pharm. Sci. 78*, 101−104.
30. Malsch, R., Guerrini, M., Torri, G., Löhr, G., Gasu, B., and Harenberg, J. (1994) *Anal. Biochem. 217*, 255−264.
31. Kay, L. E., Torchia, D. A., and Bax, A. (1989) *Biochemistry 28*, 8972−8979.
32. Farrow, N. A., Muhandiram, R., Singer, A. U., Pascal, S. M., Kay, C. M., Gish, G., Shoelson, S. E., Pawson, T., Forman-Kay, J. D., and Kay, L. E. (1994) *Biochemistry 33*, 5984−6003.
33. Lipari, G., and Szabo, A. (1982) *J. Am. Chem. Soc. 104*, 4546−4559.
34. Mandel, A. M., Akke, M., and Palmer, A. G., III (1995) *J. Mol. Biol. 246*, 144−163.
35. Faham, S., Hileman, R. E., Fromm, J. R., Linhardt, R. J., and Rees, D. C. (1996) *Science 271*, 1116−1120.
36. Kelly, R. C., Jensen, D. E., and von Hippel, P. H. (1976) *J. Biol. Chem. 251*, 7240−7250.
37. Kinosaki, M., Yamaguchi, K., Murakami, A., Ueda, M., Morinaga, T., and Higashio, K. (1998) *Biochim. Biophys. Acta 1384*, 93−102.
38. Aoyama, H., Naka, D., Yoshiyama, Y., Ishii, T., Kondo, J., Mitsuka, M., and Hayase, T. (1997) *Biochemistry 36*, 10286−10291.
39. Schlessinger, J. (1979) in *Physical Chemical Aspects of Cell Surface Events in Cellular Regulation* (DeLisi, C., and Blumenthal, R., Eds.) pp 89−118, Elsevier/North-Holland, New York.
40. Mizuno, K., Inoue, H., Hagiya, M., Shimizu, S., Nose, T., Shimohigashi, Y., and Nakamura, T. (1994) *J. Biol. Chem. 269*, 1131−1136.
41. Mikhailov, D., Linhard, R. J., and Mayo, K. H. (1997) *Biochem. J. 328*, 51−61.
42. Mulloy, B., Forster, M. J., Jones, C., and Davies, D. B. (1993) *Biochem. J. 293*, 849−858.
43. Moy, F. J., Safran, M., Seddon, A. P., Kitchen, D., Böhlen, P., Aviezer, D., Yayon, A., and Powers, R. (1997) *Biochemistry 36*, 4782−4791.
44. Lyon, M., Deakin, J. A., Mizuno, K., Nakamura, T., and Gallagher, J. T. (1994) *J. Biol. Chem. 269*, 11216−11223.
45. Koradi, R., Billeter, M., and Wüthrich, K. (1996) *J. Mol. Graphics 14*, 51−55.
46. Voet, D., and Voet, J. G. (1990) *Biochemistry*, p 235, John Wiley & Sons, New York.

BI9908641